

Crystal-growth studies of natural gas clathrate hydrates using a pressurized optical cell

EUGENE A. SMELIK^{1,2,*} AND H.E. KING JR.¹

¹Exxon Research and Engineering Company, Route 22 East, Annandale, New Jersey 08801, U.S.A.

²Department of Geological and Geophysical Sciences, Princeton University, Princeton, New Jersey 08544, U.S.A.

ABSTRACT

The crystal-growth behavior of structure I (sI), structure II (sII), and structure H (sH) clathrate hydrates has been studied using a specially designed, pressurized optical cell. Single crystals of each hydrate type, methane sI, methane-propane (95%-5%) sII, and methane-methylcyclopentane sH, were grown in equilibrium with aqueous liquid + vapor \pm liquid hydrocarbon. Each structure type exhibits characteristic crystal morphology, which suggests that crystal habit in natural settings, such as sea-floor outcrops, may allow visual identification of hydrate types. In addition, the relative growth rates for different Miller planes for each crystal type were determined. The relative growth-rate schemes and resulting crystal morphology of each structure can be related to the unit-cell density distribution of the small cages in each structure. Four-phase *P-T* equilibrium data for methane-methylcyclopentane sH data were also measured using optical methods. Evaluation of these and previously published phase-equilibrium data for all three known hydrate structures strongly suggests that hydrate assemblages of coexisting sII and sH should be common in natural settings.

INTRODUCTION

Clathrate hydrates are inclusion compounds based on a three-dimensional ice-like framework of hydrogen-bonded water molecules. This framework structure creates several polyhedral cavities of various dimensions that house included, or guest molecules. In the natural environment, the guest molecules trapped in this water framework are typically hydrocarbon gases. These gases are mostly methane, ethane, propane, and isobutane; carbon dioxide; and hydrogen sulfide. These compounds are commonly referred to as gas hydrates. Clathrate hydrates also form from mixtures of water plus ethers, fluorinated hydrocarbons, and chlorinated hydrocarbons. In-depth reviews of clathrate crystal chemistry and crystallography were given by Davidson (1973), Jeffrey (1984), Sloan (1990a), Englezos (1993), and Ripmeester et al. (1994).

Naturally occurring gas hydrates have received considerable attention over the last 15 years, ever since researchers began to realize their great abundance. Hydrate stability in nature is a function of the pressure, temperature, and composition of both the gas and liquid phases. Because of these controls, natural hydrate formations are somewhat restricted in location, occurring in deep-ocean regimes and in polar regions. Deep-ocean hydrates usually occur in sediments along the outer continental slopes where water is cold enough for hydrate stabilization (e.g., Brooks et al. 1986, 1984; Davidson et al. 1986a; Kvenvolden et al. 1993; Kvenvolden and Grantz 1990). In po-

lar regions hydrates are generally associated with permafrost in offshore and onshore sediments (e.g., Cherskiy et al. 1985; Collett 1994; Kvenvolden and Grantz 1990; Makogan 1981). Recently, unusual air-clathrate hydrates were reported from about 1000 m depths in the Antarctic polar ice (Craig et al. 1993). Natural hydrate occurrences were reviewed by Kvenvolden (1993, 1988a).

From the environmental and geologic points of view, the importance of naturally occurring gas hydrates may be considered from three perspectives. First, because hydrates contain considerable methane, they represent a possible energy resource. Though the technology has not yet been developed to economically extract the methane, the known and inferred natural hydrate formations represent staggering potential energy reserves, estimated at 10^{27} – 10^{34} m³ of methane (e.g., Holder et al. 1984; Kvenvolden 1994, 1988a; MacDonald 1990a).

Second, it has been suggested that hydrates may influence atmospheric CH₄ and CO₂ levels as gas is either released or fixed by hydrates (e.g., Kvenvolden 1988b; MacDonald 1990b; Nisbet 1992). This atmospheric cycling of methane and CO₂ is thought to have influenced climate conditions and the advance and retreat of glaciation throughout geologic time (e.g., Kvenvolden 1988b; MacDonald 1990b; Nisbet 1990; Sloan et al. 1992; Paull et al. 1991).

Third, the existence and behavior of natural hydrates may play an important role in geologic processes, such as turbidity flows of unconsolidated submarine sediments (e.g., McIver 1977, 1982), sediment slumping and slope instability along continental margins (e.g., Carpenter

* Present address: Molten Metal Technology, Inc., 421 Currant Rd., Fall River, Massachusetts 02720, U.S.A.

TABLE 1. Crystal-chemical data for water-clathrate hydrates

Structure type	Space group and cell parameters (Å)	Cage types per unit cell (letter code)*					Ideal stoichiometry	Structure references**
		5 ¹² (D)	5 ¹² 6 ² (T)	5 ¹² 6 ⁴ (H)	4 ³ 5 ⁶ 6 ³ (D')	5 ¹² 6 ⁸ (E)		
sI	<i>Pm3n</i> (227) <i>a</i> = 12.0	2	6	—	—	—	2D·6T·46H ₂ O	(McMullan and Jeffrey 1965)
sII	<i>Fd3m</i> (223) <i>a</i> = 17.3	16	—	8	—	—	16D·8H·136H ₂ O	(Mak and McMullan 1965, Davidson et al. 1986b, McMullan and Kvick 1990)
sH	<i>P6/mmm</i> (191) <i>a</i> = 12.3 <i>c</i> = 10.2	3	—	—	2	1	3D·2D'·1E·34H ₂ O	(Gerke and Gies 1984, † Ripmeester et al. 1987, Ripmeester and Ratcliffe 1990)

* N^m superscript notation describes a cage with m total faces with N edges each. For example, 5¹² indicates a cage with 12 five-sided faces (a pentagonal dodecahedron), whereas 5¹²6⁸ denotes a cage with 12 pentagonal faces and eight hexagonal faces.

** References for structure refinements or lattice measurements only.

† Structure refinement for dodecasil 1H, which is isostructural with sH hydrate.

1981; Kayen and Lee 1991), and submarine mud volcanoes (e.g., Ginsburg et al. 1992; Reed et al. 1990).

In addition to these environmental and geologic aspects of hydrates, there has been considerable interest and research in gas hydrates by the oil and gas industry since about 1940. This stems from the considerable economic impact of gas hydrate formation in both drilling and exploration operations and in pipeline-transport operations (e.g., Barker and Gomez 1989; Lingelem and Majeed 1992; Lingelem et al. 1994; Ouar et al. 1992).

In terms of H₂O clathrates, three main crystal structures have been identified. These are known as structures I (sI), II (sII), and H (sH). Structures I and II are cubic structures and were first identified in the early 1950s (Claussen 1951a, 1951b; Müller and von Stackelberg 1952; Pauling and Marsh 1952; von Stackelberg and Müller 1951). Structure H is hexagonal and was first described by Ripmeester et al. (1987). This hydrate structure is thought to be isostructural with dodecasil 1H clathrasil (Gerke and Gies 1984), a framework-guest structure with SiO₄ tetrahedral groups forming hydrate-like cages. A single-crystal structure refinement has yet to be performed for sH hydrate. Crystallographic and crystal-chemical data for these three hydrate structures are summarized in Table 1.

Knowledge of the crystal chemistry, crystallography, and stability of these three hydrate structures has been obtained from a variety of experimental and theoretical techniques, including X-ray and neutron diffraction, various spectroscopies (NMR, IR, FTIR), mathematical and thermodynamic modeling, and phase-equilibrium studies. In most of the experimental work on hydrates, the presence of hydrate crystals, or the onset of hydrate formation, has been demonstrated either by the uptake of the hydrate former, typically a gas (usually measured as a decrease in pressure); by the observation of turbidity in the solution; or by the appearance of diffraction maxima in the case of X-ray or neutron-scattering experiments.

Optical microscopy has not been fully exploited in hydrate research. Optical studies provide an opportunity to examine several macroscopic properties of gas hydrate crystals. These include crystal-growth behavior, equilibrium crystal morphologies of different hydrate structures,

and determination of relative growth rates of specific crystallographic planes or directions. In this paper we describe a pressurized optical cell designed for the study of natural gas hydrates and present optical data for each of the three naturally occurring hydrate structures.

Our main goal is to provide a visual framework to aid in the identification of unknown clathrate hydrate samples. This holds potential for in situ identification of specific hydrate phases in their natural environments, complementing the usual characterization method of evolved gas analysis from samples returned to the laboratory. As shown below, the crystal forms characteristic of each hydrate structure are distinctive. In addition, phase-equilibrium data, obtained from freezing-melting experiments, are presented for sH hydrate in the methane-methylcyclopentane-water system. This hydrate structure, only recently found in a natural environment (Sassen and MacDonald 1994), can scavenge large hydrocarbon molecules not found in sI and sII. The phase-equilibrium data for several sH hydrates suggests that their natural occurrence may be widespread.

EXPERIMENTAL METHOD

Description of experimental set-up

For the optical study of gas hydrates, a special cell was designed that enabled pressure and temperature control. A schematic diagram of the cell is shown in Figure 1. The cell consists of a ½ in. thick stainless steel body with a ½ in. bore in the center, which is the actual sample chamber.

Cooling was achieved using a Neslab RTE 140D continuous circulation chiller, which pumped a 50-50 mixture of ethylene glycol-water through insulated lines to the optical cell, where it flowed through ¼ in. ports that surround the sample chamber. The temperature range encountered in our experiments was from 256 to 290 K. Because of the relatively large volume of coolant in the chiller bath, about 7.0 L, temperature changes in the cell were gradual, rather than instantaneous; however, excellent temperature stability was achievable. The temperature was measured using a YSI model 44011 precision

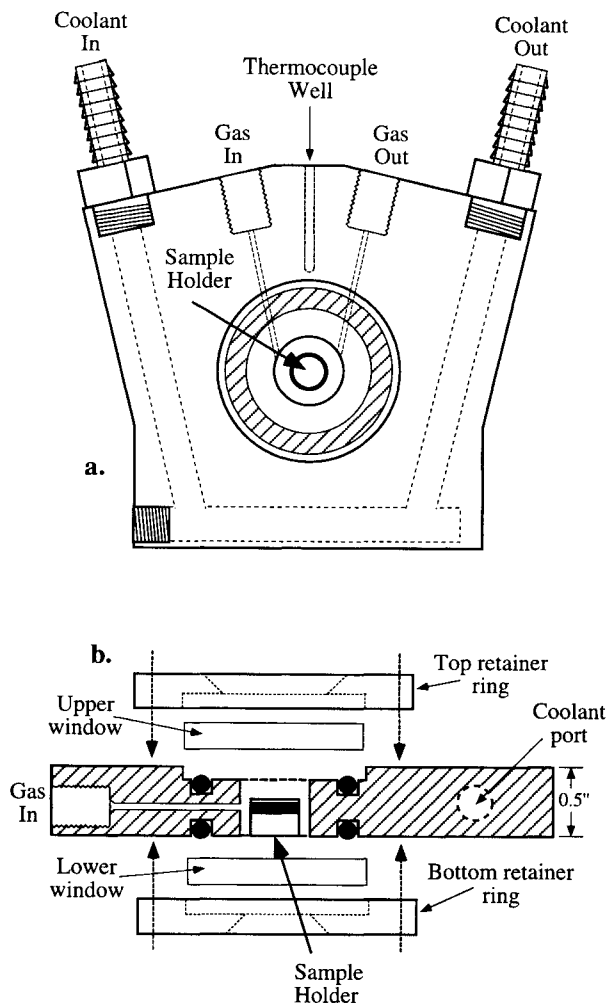


FIGURE 1. Schematic diagram of the pressurized optical cell. (a) Top view showing stainless steel body of cell with central, cylindrical sample chamber. (b) Side view showing upper and lower SiO₂ glass windows with o-ring seals and steel retainer rings. The sample holder is a small, cylindrical cup into which water is placed. It is topped by a water-impermeable, gas-permeable layer of hydrocarbon liquid. In both parts bolt holes were left out for clarity.

thermistor, which was inserted into a well in the side wall of the stainless steel body, placing the thermistor tip within a few millimeters of the sample chamber wall. Calibration experiments with sI methane hydrate showed that the temperature of the cell body matched the temperature within the sample chamber to within ± 0.4 K.

For optical viewing, the central, cylindrical, sample chamber has $\frac{3}{16}$ in. thick upper and lower SiO₂ glass windows. These are sealed with o-ring seals and held in place by stainless steel retaining rings. The upper window is slightly recessed into the cell body to allow for focusing in the bottom of the cell.

Two small ports for gas flow also lead into the sample chamber. These were connected to standard bottled gases

by $\frac{1}{16}$ in. flexible, high-pressure, stainless steel tubing connected to a pressure-control gas manifold. The highest attainable pressures were those of the bottled gases. In these experiments we used two commercially available gases: a 6000 psi (~ 40 MPa) methane (CP grade) and a 2000 psi (~ 14 MPa) mixture of 95.41% methane–4.59% propane (Me₉₅Pr₅). For sH we used liquid methylcyclopentane (Fluka AG >99% pure). Pressure was measured using a Heise model 623 pressure gauge accurate to $\pm 1\%$. All the crystal-growth experiments were conducted at pressures between about 1 and 10 MPa.

The entire optical cell was encased inside a 4.5 in. diameter, horizontally split shell composed of Delrin. This shell, about 3 in. thick, served to insulate the steel body of the optical cell for excellent temperature stability. Special ports were built into the insulating shell to allow N₂ gas flow over the upper and lower windows to prevent condensation when working at temperatures below about 278 K.

The optical microscope was an Olympus model BH-2 equipped with a polarizer and analyzer, and an x-y translation stage. A special spacer was installed in the microscope stand to allow clearance for the optical cell assembly. Normal viewing was accomplished using transmitted, plane-polarized, and crossed-polarized light. Because of the thickness of the optical cell, we used Mitutoyo M Plan APO long-working-distance objective lenses (5 \times , 20 \times , 50 \times). All images were recorded on video tape with a Sony model DXC-151 color CCD camera and a VCR. Selected images were captured using a RasterOps 24M \times TV 24-bit video card on a Macintosh computer.

Experimental procedure

Experiments were conducted by simply filling about one-half of the sample chamber with deionized water. After sealing the cell, gas was flushed through the chamber to drive out any trapped air. Using the gas-manifold controls, the pressure was then increased to the desired level. Once pressure was attained, the temperature was decreased until hydrate formed in the cell. One characteristic element of all our experiments is that because the system is essentially clean, with only deionized water and gases, and is static, a large degree of undercooling was necessary before any freezing would take place. Depending on the pressure, the thermal stability of gas hydrates is typically in the 273–293 K range. Undercooling to approximately 264–258 K was necessary to cause freezing in the cell. In all cases, this initial freezing event was rapid and usually consisted of dendritic hydrates forming at the water-gas interface. In many experiments, ice would crystallize at the same time as the hydrate. Once crystallized material formed, the temperature was increased to >273 K, depending on the pressure, so that any ice in the cell would melt, leaving only the hydrate phase.

The actual crystal-growth experiments were performed by slowly melting the dendritic hydrate material until only small, scattered hydrate crystals remained in the cell.

We have termed these “melt nuclei.” These melt nuclei then served as the primary sites for new crystal growth, once temperature was decreased, or pressure increased.

The best results were obtained by placing the liquid solutions into a plastic, cylindrical, glass-bottomed cup (isolating it from the cold side walls) and applying a thin layer of light hydrocarbon oil (two to three drops of decane, $C_{10}H_{22}$) on top of the water. This oil is not a hydrate former and serves to prevent the water from migrating out of the cup toward the coldest regions in the cell during crystallization, which would normally lead to hydrate formation in undesirable regions of the cell (i.e., along the cold side walls). In the case of sH, the decane was not used because the sH component, methylcyclopropane, served the same purpose.

EXPERIMENTAL RESULTS

Surface crystallization

Hydrates form from a mixture of water and natural gas, plus or minus other complex liquid or gas hydrocarbons. Inherent in any system of this sort is the existence of a water-gas interface. In a turbulent system, like a pressurized, flowing, natural gas pipeline, these interfaces are probably manifested as bubble surfaces or as interfaces between larger gas pockets and water. In either case, the interface area and geometry probably change continuously with time.

In our optical cell, there is a static, stratified system of water, a thin layer of oil, and gas. Once the system is pressurized, there is minimal movement of the gas and the liquid. This static arrangement produces a relatively large, unchanging water-gas interface ($\sim 50 \text{ mm}^2$), where water has its easiest access to hydrocarbon gas. As expected, hydrate-surface crystallization was a common process during supercooling. These surface textures are described first.

As mentioned above, the initial stage of any experiment involved supercooling the system until rapid freezing took place. The initial hydrates that formed were typically branching dendrites or very-fine-grained crystals, and these were not extensively characterized. Once this system melted back, leaving only small melt nuclei, temperature was slowly decreased until crystal growth was observed, usually occurring within 1 or 2 °C of the equilibrium curve. For the pure methane system (sI) and the $\text{Me}_{95}\text{Pr}_5$ system (sII), surface crystallization was ubiquitous, whereas methane-methylcyclopentane sH did not exhibit surface crystallization.

Surface crystallization proceeded in one of two ways. Commonly, large surface crystals would grow from a single melt nucleus or a nuclei cluster at the water surface. These crystals usually showed a hexagonal crystal shape and grew outward from the central nucleus (Figs. 2a and 2b). The rough-looking surfaces and movements of these crystals clearly indicated that they were floating at the water-gas interface. Eventually these surface crystals would increase in size until they impinged on one another,

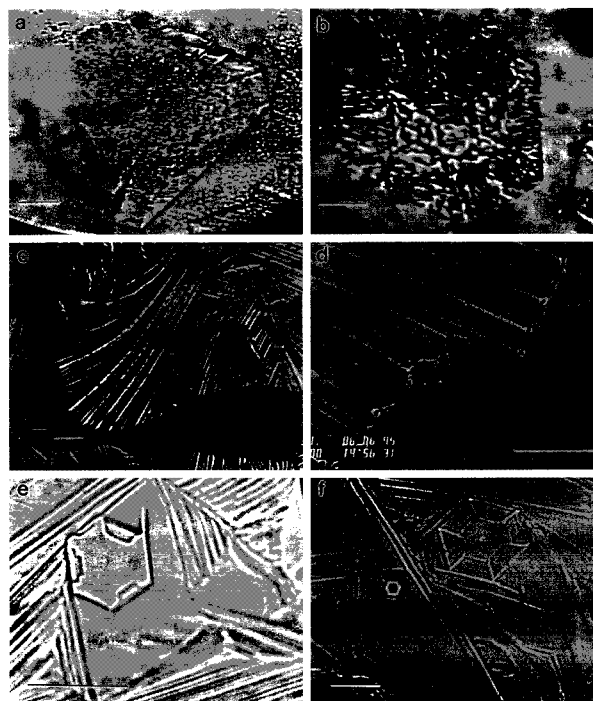


FIGURE 2. Optical images of surface crystallization for sI and sII hydrates. (a and b) Large individual surface crystals of sII hydrate, which have nucleated from small melt nuclei that were floating in the aqueous phase (see a). Their rough surface texture is due to growth at the water-gas interface. (c) Surface fronts of drapery-like sII crystallization growing across the water-gas interface. (d) High-magnification view of sI surface crystallization, showing how the surface domains are sutured together. (e and f) Two views of the complex surface mosaic for sII hydrate in which individual hexagonal-shaped hydrate crystals have become trapped in the surface mosaic. Note the unusual growth patterns for these crystals because of the proximity of the water-gas interface. Scale bars equal 50 μm .

forming a surface mosaic. A second type of surface crystallization involved several large fronts freezing across the water-gas interface simultaneously. These surface fronts commonly had a drapery appearance and almost always originated near the side walls of the cell and propagated rapidly across the cell (Fig. 2c). These fronts often met one another, becoming sutured together (Fig. 2d), or they encountered and trapped floating surface crystals until the surface was completely frozen over in a complex mosaic (Figs. 2e and 2f). The frozen hydrate surface was not flat and appeared to have considerable topography, and the thickness of this crust was always greater toward the outer rim of the sample cup. Similar surface textures were reported by Makogan (1994) for sI methane hydrate.

In large-scale hydrate systems, whether natural or industrial in origin, it is likely that surface crystallization is a common, and perhaps dominant process because of the ever-present water-gas interface. However, beyond the recognizable crystal shapes within the surface mosaic, the surface crystals themselves do not provide much infor-

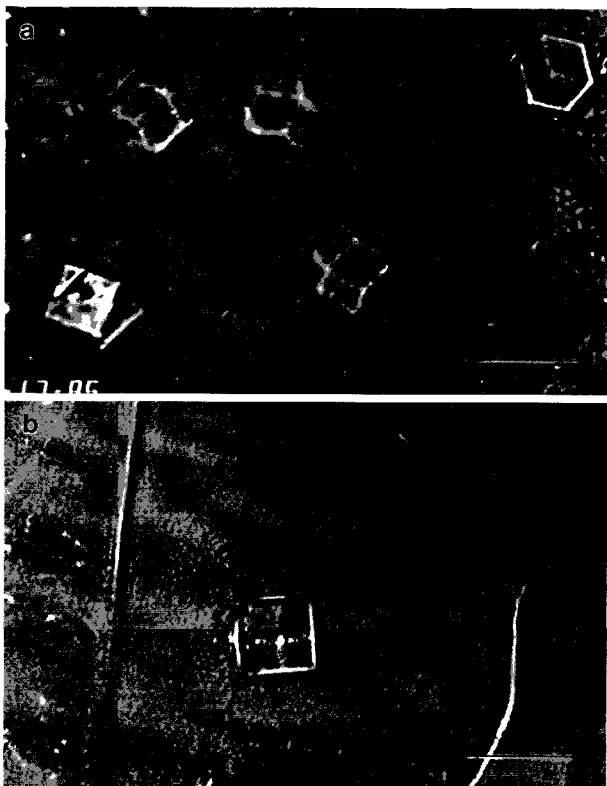


FIGURE 3. Optical images of methane sI single crystals. (a) The three central crystals are {110} rhombic dodecahedrons, the most common sI form. The crystal in the upper right appears to be a {100} cube viewed down [111], whereas in the lower left two cube-shaped crystals have formed a growth twin. (b) An example of a possible {*hhl*} trapezohedral form for sI. Note the faint cross quartering the front face of the crystal and that the side faces appear to bulge very slightly, consistent with this form. Scale bars equal 25 μm .

mation about equilibrium growth rates of different crystallographic directions or about equilibrium crystal morphologies. Despite the ubiquity of surface crystallization for sI and sII, it was possible to grow single crystals of hydrate within the bulk liquid. Because the solubility of gas in the water is low, these crystals tended to be limited in size and number. Moreover, once the water surface froze over, no additional gas could be made available for hydrate growth within the fluid unless it was able to diffuse along the suture boundaries in the mosaic.

Structure I single crystals

Cubic sI hydrate (Table 1) was grown from pure water and methane gas. Of the three structures studied, single crystals of sI methane hydrate were the most difficult to produce. We were able to grow single crystals in the bulk liquid only by continuing to cool the cell slowly after the surface mosaic had formed. Despite the presence of many melt nuclei, surface crystallization would always take place first, before any nuclei could grow into well-defined

crystals. By decreasing the temperature to about 6–8 $^{\circ}\text{C}$ below the equilibrium temperature, single crystals of methane hydrate would form in the bulk liquid below the hydrate skin, which was, fortunately, transparent enough to permit crystal investigation. These single crystals were small, never exceeding about 25 μm in diameter, and normally floated up to the underside of the hydrate surface layer.

Several cubic forms were observed, the most common being the rhombic dodecahedron. Figure 3a shows three such crystals in the central part of the image. This form consists of 20 rhombohedral (diamond-shaped) faces with {110} indices (identical to common garnet). Two other crystals are shown in Figure 3a, one is a cube, viewed down the [111] diagonal, and the other appears to be a growth twin of two cube-shaped crystals.

Another possible crystal form that was more rarely observed is the trapezohedron. This form consists of 24 trapezium-shaped faces with {*hhl*} indices. These forms were difficult to identify because of their close similarity to cubes (Fig. 3b), especially when the *h* and *l* indices are high, as they appeared to be in this case. The image in Figure 3b shows a view down the fourfold rotation axis of a cube-shaped crystal. Notice the faint cross quartering the (100) face and that the other {100} faces seem to bulge somewhat, suggesting deviation from regular cube shape.

All the sI crystals are isotropic, and the observed forms are consistent with the point-group symmetry of the sI space group.

Structure II single crystals

Cubic sII hydrate (Table 1) was grown from pure water and an Me_9Pr_5 gas mixture. Single crystals of sII within the bulk liquid could be grown in the absence of the hydrate surface skin and below the hydrate skin. Structure II occurs in two dominant morphologies, regular octahedra and thin platelets (Fig. 4). In both cases the single crystals were clearly tumbling through the host liquid and not in contact with the water-gas interface. The platelet crystals usually displayed hexagonal, trigonal, or triangular shape (Figs. 4a and 4b). In comparison with the sI crystals above, these platelets grew quite large, reaching up to 100 μm across, but were generally only a few microns thick. Occasionally, two or more platelets would become intergrown with each other, such that they were interpenetrating. Structure II hexagonal-shaped platelets have been previously described for $8\text{CCl}_4 \cdot 3.5\text{Xe} \cdot 136\text{D}_2\text{O}$ hydrate (McMullan and Kvick 1990). The large faces of the platelets are {111} planes.

The other dominant form is the regular octahedron (Figs. 4c and 4d). These crystals are about 25 μm in diameter, like the sI crystals, and are bound by regular {111} faces. These typically were found growing in the bulk water after the formation of a hydrate surface layer. The fact that the octahedra remain small despite further decreases in temperature, attests to the low solubility of gas in the water. The platelets and octahedra were nor-

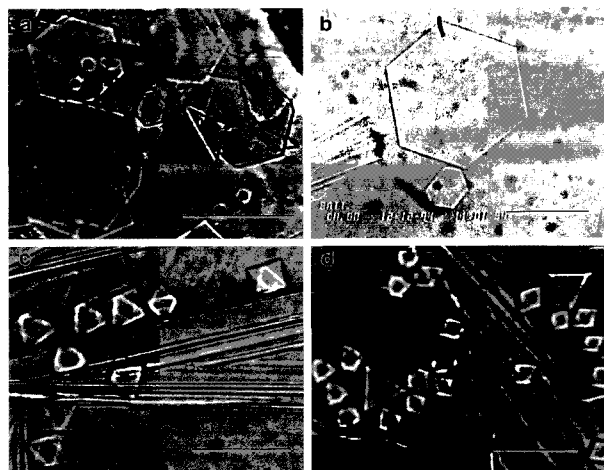


FIGURE 4. Optical images of $\text{Me}_{95}\text{Pr}_5$ sII single crystals. (a) Cluster of thin individual platelet crystals. These typically had hexagonal, trigonal, or triangular shape, bound by large $\{111\}$ faces, and were clearly drifting in the bulk liquid. (b) A pair of hexagonal platelets near the water-gas interface, about to be engulfed by the advancing surface crystallization front from the left. (c and d) Two views of clusters of perfect $\{111\}$ octahedra of sII hydrate existing in the bulk liquid below the frozen hydrate crust. These octahedra were remarkably uniform in size, reaching a maximum diameter of about $25\ \mu\text{m}$. In d, triangular platelets can also be seen with the octahedra. Scale bars equal $50\ \mu\text{m}$.

mally found growing together, suggesting one form is not preferred over the other.

Structure H single crystals

Structure H is the most recently discovered hydrate structure (Ripmeester et al. 1987). From a combination of powder X-ray diffraction data and NMR spectroscopic data (Ripmeester and Ratcliffe 1990; Ripmeester et al. 1987; Tse 1990), sH appears to be hexagonal $P6/mmm$ (Table 1) and is isostructural with dodecasil 1H clathrasil (Gerke and Gies 1984). Our optical observations are consistent with this model.

On the basis of the work of Ripmeester and Ratcliffe (1990), we chose methylcyclopentane, C_6H_{12} , as the hydrate former, in addition to deionized water and pure methane gas. In these experiments the methylcyclopentane was added to the top of the water in the sample cup, after which the system was pressurized with methane gas. The initial freezing event always resulted in the formation of both sI and sH. Once the sI methane hydrate melted, single crystals of sH could be grown from the stable sH melt nuclei scattered throughout the cell.

The predominant crystal form for sH is the hexagonal prism (Figs. 5a and 5b). These beautiful six-sided prismatic crystals grew in all sizes and orientations within the cell. The majority of the crystals would lie flat, however, along the water-hydrocarbon interface. Being hexagonal, the crystals could be studied in crossed-polarized light (Fig. 5b). The thicker crystals showed strong

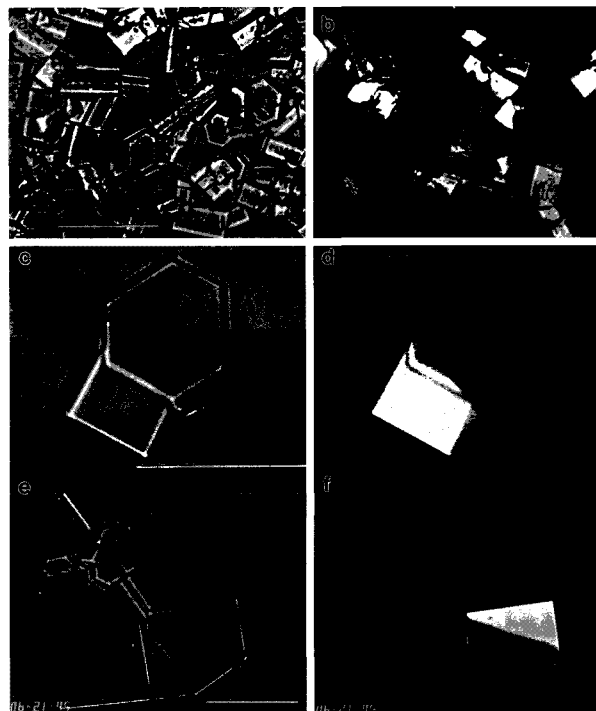


FIGURE 5. Optical images of methane-methylcyclopentane sH single crystals. (a) Plane-light view of a cluster of hexagonal prisms, the most common crystal form for sH. (b) Crossed-polarized-light view of similar area showing anisotropic character of these hexagonal crystals. All the crystals have parallel extinction. (c and d) Example of a growth twin involving two well-formed hexagonal prisms. Part d is the crossed-polarized-light view with the crystal in the (001) orientation fully extinct. Note that the twin boundary is not planar, but curved. (e) Mixture of hexagonal prisms, one quite long, and a different type of common growth twin, involving two rectangular platelet crystals. The crossed-polarized-light view of this coarsened twin in f reveals that the twin plane may not be vertical. Scale bars equal $50\ \mu\text{m}$.

birefringence, and all the prismatic crystals showed parallel extinction, consistent with hexagonal symmetry. There were many examples of distorted hexagonal prisms and combinations with other forms as well.

Growth twins were also common in this system (Figs. 5c–5f). These typically involved intergrown hexagonal prisms (Figs. 5c and 5d) or intergrown rectangular platelets (Figs. 5e and 5f). The latter style of twinning was more common among crystals floating at the water surface. The intergrowth plane for the prismatic twins tended to be irregular in shape and orientation (Fig. 5d), whereas the twin plane for the platelet twins always nearly bisected the obtuse angle created by the two individuals (Fig. 5f).

Because the rectangular platelet twins were common, a possible crystallographic description of this intergrowth can be presented. Because the twinned crystals show birefringence, the large flat face parallel to the plane of the image cannot be (001). Each crystal in a twinned pair

shows two faces at 90° to each other (Fig. 5e). It is likely that these two faces have indices of the sort (00*l*) and (*hk*0), respectively. On the basis of parallel extinction criteria, we assumed that these two faces are (001) and (100), respectively. Given this assumption, it follows that the large flat face, normal to these other two, is (120) and that the view is down the *b* axis or [010] zone. If the twin plane is vertical, in the [010] zone, then it must be of the sort {*h*0*l*}. The obtuse angle between the two twin individuals is about 116°. If the unit cell of Ripmeester and Ratcliffe (1990) is used, the angle between (001) and (503) is 57.92° (~116 ÷ 2), making it the best candidate. If the twin plane is not in the [010] zone, as the unusual birefringence in Figure 5f might suggest, then it probably has a relatively high *k* index.

Phase-equilibrium data for structure H

The phase behavior of hydrate systems involving light hydrocarbons and water is complex. This is largely because of the low mutual solubility between the water and the hydrocarbon phase(s) and because of the formation of the solid hydrate compound itself [see review by Harmens and Sloan (1990) describing the important aspects of these kinds of systems]. A thorough understanding of the phase behavior of hydrate systems is of critical importance, however, especially in light of the potential environmental impact represented by the behavior of natural hydrates and the costly hydrate-related problems that plague the natural gas and petroleum industry.

Phase-equilibrium data for sI and sII hydrates are readily available in the literature (e.g., Deaton and Frost 1946; Parrish and Prausnitz 1972 and references therein). Excellent reviews of the natural gas phase equilibria of these hydrate types were provided by Sloan (1990b) and Holder et al. (1988).

Over the last few years, phase-equilibrium data for sH hydrates have begun to appear in the literature. To date, experimental phase-equilibrium data for sH has been reported by Lederhos et al. (1992) for the system water-methane-adamantane, by Mehta and Sloan (1993) for the systems methane + 2,2-dimethylbutane, methane + 2-methylbutane, and methane + methylcyclohexane, and by Thomas and Behar (1994) for several systems containing methane and larger hydrocarbons, including methylcyclopentane, the large hydrocarbon used in this study.

To evaluate the usefulness of our optical cell for phase-equilibrium measurements, we determined equilibrium *P-T* points for methane-methylcyclopentane sH. The determination of these points was accomplished by holding the cell at various constant temperatures and changing the pressure while observing either the growth or melting of the hydrate crystals. Because pressure changes are achieved by varying line pressure, they occur nearly instantaneously throughout the small volume of the cell. One of the difficulties in determining optically the exact equilibrium points is that the reaction rates are very slow very near the phase boundary. Each point was bracketed by cycling up and down in pressure and allowing the

TABLE 2. Phase-equilibrium *P-T* points for sI and sH hydrates determined using the optical cell

Methane sI		Methane-methylcyclopentane sH	
<i>T</i> (K)	<i>P</i> (kPa)	<i>T</i> (K)	<i>P</i> (kPa)
273.0	2482	275.3	2400
276.2	3493	276.4	2730
278.8	4426	277.4	2813
279.9	5130	278.1	3177
281.9	6205	278.9	3228
284.5	8356	280.5	3900
		282.1	4990
		282.2	4800
		282.9	5014
		283.1	5502

assemblage to sit for up to 45 min to see whether melting or growth occurred. As the equilibrium phase boundary was closely approached, the assemblage remained unchanged for longer periods of time.

The same procedure was followed for several temperatures in the pure methane system (sI). Comparison with previous data for methane sI hydrate (Deaton and Frost 1946) and methane-methylcyclopentane sH hydrate (Thomas and Behar 1994) indicates that this technique is an accurate means of determining phase equilibria. The four-phase equilibrium ($L_w + H + V + L_{HC}$) *P-T* points for methane-methylcyclopentane sH hydrate and for pure methane sI hydrate ($L_w + H + V$) are summarized in Table 2.

DISCUSSION

Relative growth rates of crystal forms

The results presented above indicate that single crystals of all three known hydrate structures can be easily grown in the laboratory for optical study. Other results of optical studies have been published, mostly by Russian researchers (Makogan 1994), but these results focused more on surface-crystallization textures at the water-gas interface and whisker crystals forming within the gas medium, and more recently some crystal-morphology results were presented by Larsen et al. (1996). For crystals coexisting with liquid, each hydrate type exhibits different morphology. This observation suggests that optical examination may be potentially very useful for the rapid identification of natural hydrates collected in the field, instead of gas extraction and analysis or other more involved techniques (e.g., Brooks et al. 1984; Davidson et al. 1986a). In light of recent excursions by deep-sea submarines to natural hydrate zones (Sassen and MacDonald 1994), perhaps the vessels could be outfitted such that optical identification could be performed in situ, eliminating the problem of preserving and transporting the hydrate samples.

The observed crystal morphologies allow the evaluation of relative growth rates for different crystallographic planes or directions for each hydrate type. In conducting this analysis, it is important to recall that under ideal conditions the bounding faces of any crystal generally cor-

TABLE 3. Unit-cell distribution of small cages in sI, sII, and sH

Miller plane	Structure I*	Structure II*	Structure H**
{h00}	4	7	6
{hh0}	5	8	4
{hhh}	3	12	1
{00l}	n.a.	n.a.	5

Note: n.a. = not applicable.
 * Only 5¹² cages.
 ** Includes both small cages: 5¹² and 4³5⁶3.

respond to the slowest growing directions or planes, whereas the fastest growing directions typically never develop corresponding morphologic faces and instead occur as apices or edges of the crystal.

For methane sI hydrate, the common rhombic dodecahedral form, bounded by {110} faces (Fig. 3a), suggests that the {110} planes are the slowest growing, whereas growth along the crystallographic axes ({h00} planes) and along [111] (the cubic diagonal) is more rapid. Because {100} cubes and possible {hhl} trapezohedrons were also sometimes observed, but {111} octahedra were not seen, the relative growth rates for the primary crystallographic planes of sI hydrates can be given as {111} > {100} > {110}.

This is in contrast with sII hydrates, for which the regular {111} octahedron was a common form, or hexagonal platelets with large {111} faces (Fig. 4). These observations suggest that the {111} planes are the slowest growing. Work by Smelik and King (unpublished) on sII THF-water hydrates has provided many examples of distorted {111} octahedral forms containing {110} edges. Cube-shaped crystals or rhombic dodecahedra were not observed. These combined observations give the following relative growth rates for crystallographic planes in sII hydrates: {100} > {110} > {111}.

It should be possible to reconcile these different relative growth-rate schemes and morphologies in terms of the crystal structures of sI and sII. Structural data for sI and sII are given in Table 1, indicating that both hydrates are cubic. Hydrate structures are usually described in terms of packing or layering of face-sharing pentagonal dodecahedra ([5¹²] cages) formed by the hydrogen-bonded water molecules (e.g., Jeffrey 1984; Ripmeester et al. 1994; Smelik and King 1996). The particular way in which these basic building blocks are packed together leads to the wide array of additional cavities that are found in hydrate structures.

One may envision the growth of a hydrate crystal proceeding by the addition, through hydrogen bonding, of new water molecules to the existing three-dimensional framework. As the framework is built up in this way, guest molecules are trapped in the cages before the cages are fully closed. Because the larger cages form as a result of the packing together of the smaller, dodecahedral cages, it seems possible that the building of the [5¹²] cages is critical to the formation of the crystals. Presumably, a small crystal of hydrate immersed in water is completely

surrounded by molecules of H₂O that can be scavenged by the growing crystal. In a system like ours, which is saturated with the hydrate former (methane or Me₉₅Pr₅), it is also likely that the guest molecules are equally available to any region of the crystal. Furthermore, it is reasonable to assume that the energy required to build a new [5¹²] cage (hydrogen bonding) is constant, no matter where at the hydrate crystal surface the growth is occurring. If the construction of the [5¹²] cages is a rate-limiting factor, then there should be a correlation between the number of these cages in a given crystallographic plane and the growth rate of that plane, with planes containing a high density of [5¹²] cages growing more slowly than those with fewer cages.

By representing the [5¹²] cages by their centers, we analyzed the unit-cell density of [5¹²] cages for {h00}, {hh0}, and {hhh} planes in both sI and sII. The results are summarized in Table 3. For sI, the planes with the highest density of [5¹²] cages are, in fact, the {hh0} planes, which appear to be the slowest growing. The {hhh} planes in sI have the lowest [5¹²] density and thus grow most rapidly, consistent with the optical observations. For sII, the {hhh} planes have the highest density of [5¹²] cages, and the {h00} planes have the lowest, with {hh0} intermediate but close to {h00}. This result predicts the development of octahedral forms or distorted octahedral forms for the sII hydrates, in exact agreement with our observations. This simple correlation suggests that the relative growth rates of various planes in common hydrates, under ideal or equilibrium conditions, can be predicted by determining the density distribution of [5¹²] cages. This relationship is consistent with the periodic bond-chain (PBC) theory of crystal-habit formation presented by Hartman (1987). In the context of the PBC theory, the [5¹²] cage is the fundamental unit of the periodic bond chain.

The situation for sH is slightly more complicated because there are two distinct small cages, the [5¹²] and the [4³5⁶3]. The structure consists of a basal layer of six-membered rings of [5¹²] dodecahedra at $z = 0$, with a layer of six-membered rings of [4³5⁶3] polyhedra stacked on top of this at $z = \frac{1}{2}$. Another [5¹²] layer at $z = 1$ closes the large, asymmetric [5¹²6⁸] polyhedron, completing the unit cell (see Lederhos et al. 1992). Thus, growth of a crystal would depend on the formation of both types of small cages. A similar density-distribution analysis was performed for sH considering both types of small cages (Table 3). The results suggest that the crystals should be bound by {00l} and {h00} planes. The optical results indicated that the most common form was indeed the hexagonal prism. This form can be either a first-order {100} prism or a second-order {110} prism, which are identical in appearance. The results in Table 3 suggest that the prisms are first order because the density of small cages is less on {hh0} planes, such that they would grow faster. The aspect ratio of the prismatic sH crystals was quite variable, suggesting that the growth rates for the {h00} and {00l} families of planes are similar.

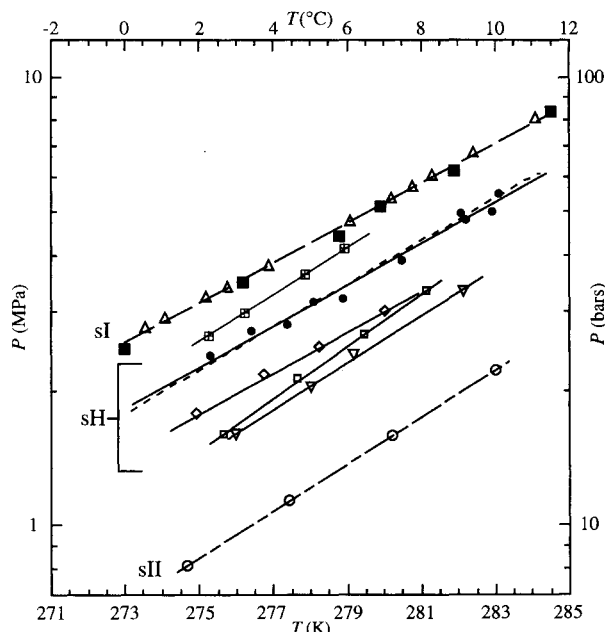


FIGURE 6. Plot of P - T equilibrium data measured for methane sI (solid squares) and methane-methylcyclopentane sH hydrate (solid circles) using the pressurized optical cell. Also shown are the data from the literature for methane sI (open triangles; Deaton and Frost 1946), $\text{Me}_{95.2}\text{Pr}_{4.8}$ sII (open circles; Deaton and Frost 1946), and several sH hydrates (crossed squares, open diamonds, open squares, and inverted open triangles, all data of Mehta and Sloan 1993). Curves for sI and sII are three-phase equilibrium lines, whereas all the sH lines are four-phase equilibrium lines. Also shown as a dashed line is the predicted location for sH hydrate based on a correlation of sI and sII P - T data with mean cavity size, given by Lederhos et al. (1993). The present results for methane-methylcyclopentane sH hydrate fall within the envelope of published sH curves and are in near exact agreement with the measured P - T equilibrium data of Thomas and Behar (1994) for this hydrate.

Some prismatic crystals had much higher aspect ratios, however, like the one shown in Figure 5e. The higher ratios may result because the large methylcyclopentane molecules, which are housed in the large, asymmetric $[5^{12}6^8]$ cages, have the easiest access to these cages along the c axis as the crystal is growing. This is because these oblong cages are stacked end to end along $[001]$, sharing their upper and lower hexagonal rings. This geometry should enhance growth along c , in comparison with all other directions.

Stability of structure H

The importance of sH in the geologic environment, and in the natural gas and petroleum industry, has yet to be fully assessed. Natural methane derived biogenically is nearly pure and therefore forms sI. The P - T stability region for sI is limited to $P > 3.5$ MPa at 277 K (Fig. 6), or ocean depth of about 350 m (using the hydrothermal gradient of Kvenvolden 1988b). However, thermogenic

natural gas is a mixture of methane, larger hydrocarbon gases, and other species (e.g., Kvenvolden 1993). As is evident from Figure 6, such gas mixtures typically form sII rather than sI. For example, at 277 K sII forms near 1.0 MPa, an ocean depth of only about 100 m. The widespread occurrence of natural sII hydrate has been confirmed by analyses of field samples from the Gulf of Mexico (Brooks et al. 1984, 1986; Davidson et al. 1986a). A recent report provides evidence for natural sH hydrate from the Gulf of Mexico continental slope (Sassen and MacDonald 1994). In the laboratory, Ripmeester and Ratcliffe (1990) identified about 25 large hydrocarbon guests capable of forming sH. These results, plus recent reports showing that sH forms from liquid hydrocarbon components in petroleum (including components of gasoline) (Thomas and Behar 1994; Sloan 1994), strongly suggest that hydrates with this structure may be more common than previously thought.

Our phase-equilibrium results for sH methane-methylcyclopentane hydrate (Table 2) are plotted in Figure 6. Also shown in Figure 6 are data points from Deaton and Frost (1946) for sI methane hydrate and for sII using $\text{Me}_{95.2}\text{Pr}_{4.8}$ gas, a mixture nearly identical to that used in this study. In addition, data for several sH systems are also shown for comparison. The phase boundary for sH methane-methylcyclopentane hydrate plots between the curves for sI and sII and is identical to that determined by Thomas and Behar (1994). The slope for methane-methylcyclopentane sH is nearly identical to that for methane sI hydrate.

The combined results for sH hydrate shown in Figure 6 show that the exact P - T locations of sH equilibrium curves are strongly dependent on the nature of the sH guest molecule. Furthermore, the data show that given a mixture of hydrocarbon gases and liquids, an assemblage of sII and sH hydrate would clearly form first, before the necessary depths or temperatures were reached to stabilize sI hydrate. These data therefore suggest that sH + sII assemblages should be common natural occurrences.

ACKNOWLEDGMENTS

We are indebted to Thomas Sun and Dudley Herschbach for many stimulating discussions, and to Mark Disko for his expertise in image processing. We thank Larry Wenzel from American Design, Stirling, N.J., for his help in designing and manufacturing the optical cell. Thorough reviews were provided by Laura Stern, Kathryn Nagy, and an anonymous reviewer, all of which improved the manuscript.

REFERENCES CITED

- Barker, J.W., and Gomez, R.K. (1989) Formation of hydrates during deep-water drilling operations. *Journal of Petroleum Technology*, 41, 297-301.
- Brooks, J.M., Kennicutt, M.C., II, Fay, R.R., and Sassen, R. (1984) Thermogenic gas hydrates in the Gulf of Mexico. *Science*, 225, 409-411.
- Brooks, J.M., Cox, H.B., Bryant, W.R., Kennicutt, M.C., II, Mann, R.G., and McDonald, T.J. (1986) Association of gas hydrates and oil seepage in the Gulf of Mexico. *Organic Geochemistry*, 10, 221-234.
- Carpenter, G. (1981) Coincident sediment slump/clathrate complexes on the U.S. Atlantic continental slope. *Geo-Marine Letters*, 1, 29-32.
- Cherskiy, N.V., Tsarev, V.P., and Nikitin, S.P. (1985) Investigation and

- prediction of conditions of accumulation of gas resources in gas-hydrate pools. *Petroleum Geology*, 21, 65–89.
- Claussen, W.F. (1951a) Suggested structures of water in inert gas hydrates. *Journal of Chemical Physics*, 19, 259–260.
- (1951b) A second water structure for inert gas hydrates. *Journal of Chemical Physics*, 19, 1425–1426.
- Collett, T.S. (1994) Permafrost-associated gas hydrate accumulations. In E.D. Sloan Jr., J. Happel, and M.A. Hnatow, Eds., *International conference on natural gas hydrates*, 715, p. 247–269. New York Academy of Sciences, New York.
- Craig, H., Shoji, H., and Langway, C.C., Jr. (1993) Nonequilibrium air clathrate hydrates in Antarctic ice: A paleopiezometer for polar ice caps. *Proceedings of the National Academy of Science U.S.A.*, 90, 11416–11418.
- Davidson, D.W. (1973) Clathrate hydrates. In F. Franks, Ed., *Water: A comprehensive treatise*, 2, p. 115–225. Plenum Press, New York.
- Davidson, D.W., Garg, S.K., Gough, S.R., Handa, Y.P., Ratcliffe, C.I., Ripmeester, J.A., and Tse, J.S. (1986a) Laboratory analysis of a naturally occurring gas hydrate from sediment of the Gulf of Mexico. *Geochimica et Cosmochimica Acta*, 50, 619–623.
- Davidson, D.W., Handa, Y.P., Ratcliffe, C.I., Ripmeester, J.A., Tse, J.S., Dahn, J.R., Lee, F., and Calvert, L.D. (1986b) Crystallographic studies of clathrate hydrates: Part I. Molecular Crystals Liquid Crystals, 141, 141–149.
- Deaton, W.M., and Frost, E.M., Jr. (1946) Gas hydrates and their relation to the operation of natural-gas pipe lines. U.S. Bureau of Mines Monograph, 8, p. 101, Department of the Interior.
- Englezos, P. (1993) Clathrate hydrates. *Industrial and Engineering Chemistry Research*, 32, 1251–1274.
- Gerke, H., and Gies, H. (1984) Studies on clathrasils: IV. Crystal structure of dodecasil 1H, a synthetic clathrate compound of silica. *Zeitschrift für Kristallographie*, 166, 11–22.
- Ginsburg, G.D., Guseynov, R.A., Dadashev, A.A., Ivanov, G.A., Kazantsev, S.A., Soloviev, V.A., Telepnev, E.V., Askeri-Nasirov, R.Y., Yesikov, A.D., Mal'tseva, V.I., Mashirov, Y.G., and Shabayeva, I.Y. (1992) Gas hydrates of the southern Caspian. *International Geology Review*, 34, 765–782.
- Harmens, A., and Sloan, E.D., Jr. (1990) The phase behavior of the propane-water system: A review. *Canadian Journal of Chemical Engineering*, 68, 151–158.
- Hartman, P. (1987) Modern PBC theory. In I. Sunagawa, Ed., *Morphology of crystals*, p. 271–319. Reidel, Boston.
- Holder, G.D., Kamath, V.A., and Godbole, S.P. (1984) The potential of natural gas hydrate as an energy resource. *Annual Review of Energy*, 9, 427–445.
- Holder, G.D., Zetts, S.P., and Paradhan, N. (1988) Phase behavior in systems containing clathrate hydrates. *Reviews in Chemical Engineering*, 5, 1–70.
- Jeffrey, G.A. (1984) Hydrate inclusion compounds. In J.L. Atwood, J.E.D. Davies, and D.D. MacNicol, Eds., *Inclusion compounds*, 1, p. 135–190. Academic Press, New York.
- Kayen, R.E., and Lee, H.J. (1991) Pleistocene slope instability of gas hydrate-laden sediment on the Beaufort Sea margin. *Marine Geotechnology*, 10, 125–141.
- Kvenvolden, K.A. (1988a) Methane hydrate: A major reservoir of carbon in the shallow geosphere? *Chemical Geology*, 71, 41–51.
- (1988b) Methane hydrates and global climate. *Global Biogeochemical Cycles*, 2, 221–228.
- (1993) Gas hydrates: Geological perspective and global change. *Reviews in Geophysics*, 31, 173–187.
- (1994) Natural gas hydrate occurrence and issues. In E.D. Sloan Jr., J. Happel, and M.A. Hnatow, Eds., *International conference on natural gas hydrates*, 715, p. 232–246. New York Academy of Sciences, New York.
- Kvenvolden, K.A., and Grantz, A. (1990) Gas hydrates of the Arctic Ocean region. In *The geology of North America*, L, p. 539–549. The Geological Society of America, Boulder.
- Kvenvolden, K.A., Ginsburg, G.D., and Soloviev, V.A. (1993) Worldwide distribution of subaquatic gas hydrates. *Geo-Marine Letters*, 13, 32–40.
- Larsen, R., Makogan, T.Y., Knight, C.A., and Sloan, E.D., Jr. (1996) The influence of kinetic inhibitors on the morphology of sI and sII clathrate hydrates. In *Proceedings of the second international conference on natural gas hydrates*, Toulouse, France, June 2–6, 1996, p. 163–170.
- Lederhos, J.P., Mehta, A.P., Nyberg, G.B., Warn, K.J., and Sloan, E.D., Jr. (1992) Structure H clathrate hydrate equilibria of methane and adamantane. *American Institute of Chemical Engineers Journal*, 38, 1045–1048.
- Lederhos, J.P., Christiansen, R.L., and Sloan, E.D., Jr. (1993) A first order method of hydrate equilibrium estimation and its use with new structures. *Fluid Phase Equilibria*, 83, 445–454.
- Lingelem, M.N., and Majeed, A.I. (1992) Hydrate formation and control in long distance submarine pipelines. *Transactions of the Institution of Chemical Engineers*, 70, 38–42.
- Lingelem, M.N., Majeed, A.I., and Stang, E. (1994) Industrial experience in evaluation of hydrate formation, inhibition, and dissociation in pipeline design and operation. In E.D. Sloan Jr., J. Happel, and M.A. Hnatow, Eds., *International conference on natural gas hydrates*, 715, p. 75–93. New York Academy of Sciences, New York.
- MacDonald, G.J. (1990a) Role of methane clathrates in past and future climates. *Climatic Change*, 16, 247–281.
- (1990b) The future of methane as an energy resource. *Annual Review of Energy*, 15, 53–83.
- Mak, T.C.W., and McMullan, R.K. (1965) Polyhedral clathrate hydrates: X. Structure of the double hydrate of tetrahydrofuran and hydrogen sulfide. *Journal of Chemical Physics*, 42, 2732–2737.
- Makogan, Y.F. (1981) *Hydrates of natural gas*, 237 p. Pennwell, Tulsa.
- (1994) Russia's contribution to the study of gas hydrates. In E.D. Sloan Jr., J. Happel, and M.A. Hnatow, Eds., *International conference on natural gas hydrates*, 715, p. 119–160. New York Academy of Sciences, New York.
- McIver, R.D. (1977) Hydrates of natural gas: Important agent in geologic processes (abstr). *Geological Society of America Abstracts with Programs*, 9, 1089–1090.
- (1982) Role of naturally occurring gas hydrates in sediment transport. *American Association of Petroleum Geologists Bulletin*, 66, 789–792.
- McMullan, R.K., and Jeffrey, G.A. (1965) Polyhedral clathrate hydrates: IX. Structure of ethylene oxide hydrate. *Journal of Chemical Physics*, 42, 2725–2732.
- McMullan, R.K., and Kvik, Å. (1990) Neutron diffraction study of the structure II clathrate hydrate: 3.5Xe·8CCl₄·136D₂O at 13 and 100 K. *Acta Crystallographica*, B46, 390–399.
- Mehta, A.P., and Sloan, E.D., Jr. (1993) Structure H hydrate phase equilibria of methane + liquid hydrocarbon mixtures. *Journal of Chemical Engineering Data*, 38, 580–582.
- Müller, H.R., and von Stackelberg, M. (1952) Zur struktur der gas hydrate. *Naturwissenschaften*, 39, 20–21.
- Nisbet, E.G. (1990) The end of the Ice-Age. *Canadian Journal of Earth Sciences*, 27, 148–157.
- (1992) Sources of atmospheric CH₄ in early postglacial time. *Journal of Geophysical Research*, 97, 12859–12867.
- Ouar, H., Cha, S.B., Wilderman, T.R., and Sloan, E.D., Jr. (1992) The formation of natural gas hydrates in water-based drilling muds. *Transactions of the Institution of Chemical Engineers*, 70, 48–54.
- Parrish, W.R., and Prausnitz, J.M. (1972) Dissociation pressures of gas hydrates formed by gas mixtures. *Industrial Engineering Chemical Process Design and Development*, 11, 26–35.
- Pauling, L., and Marsh, R.E. (1952) The structure of chlorine hydrate. *Proceedings of the National Academy of Sciences U.S.A.*, 38, 112–118.
- Paull, C.K., Ussler, W., III, and Dillon, W.P. (1991) Is the extent of glaciation limited by marine gas-hydrates? *Geophysical Research Letters*, 18, 432–434.
- Reed, D.L., Silver, J.E., Tagudin, J.E., and Shipley, T.H. (1990) Relations between mud volcanoes, thrust deformation, slope sedimentation, and gas hydrate, offshore north Panama. *Marine Petroleum Geology*, 7, 44–54.
- Ripmeester, J.A., Tse, J.S., Ratcliffe, C.I., and Powell, B.M. (1987) A new clathrate hydrate structure. *Nature*, 325, 135–136.
- Ripmeester, J.A., and Ratcliffe, C.I. (1990) ¹²⁹Xe NMR studies of clathrate

- hydrates: New guests for structure II and structure H. *Journal of Physical Chemistry*, 94, 8773–8776.
- Ripmeester, J.A., Ratcliffe, C.I., Klug, D.D., and Tse, J.S. (1994) Molecular perspectives on structure and dynamics in clathrate hydrates. In E.D. Sloan Jr., J. Happel, and M.A. Hnatow, Eds., *International conference on natural gas hydrates*, 715, p. 161–176. New York Academy of Sciences.
- Sassen, R., and MacDonald, I.R. (1994) Evidence for structure H hydrate, Gulf of Mexico continental slope. *Organic Geochemistry*, 22, 1029–1032.
- Sloan, E.D., Jr. (1990a) *Clathrate hydrates of natural gases*, 365 p. Marcel Dekker, Inc., New York.
- (1990b) Natural gas hydrate phase equilibria and kinetics: Understanding the state-of-the-art. *Revue de L'Institut Francais du Petrole*, 45, 245–266.
- (1994) Conference overview. In E.D. Sloan Jr., J. Happel, and M.A. Hnatow, Eds., *International conference on natural gas hydrates*, 715, p. 1–23. New York Academy of Sciences, New York.
- Sloan, L.C., Walker, J.C.G., Moore, T.C., Jr., Rea, D.K., and Zachos, J.C. (1992) Possible methane-induced polar warming in the early Eocene. *Nature*, 357, 320–322.
- Smelik, E.A., and King, H.E., Jr. (1996) Clathrate hydrates as layer structures: Comparison between the structures of type II and hypothetical type V. *Zeitschrift für Kristallographie*, 211, 84–89.
- Thomas, M., and Behar, E. (1994) Structure H hydrate equilibrium of methane and intermediate hydrocarbon molecules. *Proceedings of the Annual Convention on Gas Processes Association*, 73, 100–107.
- Tse, J.S. (1990) Thermal expansion of structure-H clathrate hydrates. *Journal of Inclusion Phenomena and Molecular Recognition in Chemistry*, 8, 25–32.
- von Stackelberg, M., and Müller, H.R. (1951) On the structures of gas hydrates. *Journal of Chemical Physics*, 19, 1319–1320.

MANUSCRIPT RECEIVED APRIL 16, 1996

MANUSCRIPT ACCEPTED OCTOBER 9, 1996